A Robust Algorithm for Automatic Target Recognition Using Passive Radar

Lisa M. Ehrman and Aaron D. Lanterman
Center for Signal and Image Processing
School of Electrical and Computer Engineering
Georgia Institute of Technology
Mail Code 0250, Altanta, GA 30332
ehrman@ece.gatech.edu, lanterma@ece.gatech.edu

Abstract — The goal of this research is to add automatic target recognition (ATR) capabilities to existing passive radar systems. We do so by comparing the radar cross section (RCS) of detected targets to the precomputed RCS of known targets in the target class. The precomputed RCS of the targets comprising the target class is modeled using a multi-step process involving programs such as the Fast Illinois Solver Code (FISC), Advanced Refractive Effects Prediction System (AREPS), and Numerical Electromagnetic Code (NEC2). A Rician likelihood model compares the power profile of the detected target to the precomputed power profiles of the targets in the target class; this comparison results in target identification.

Thus far, the results of simulations are encouraging, indicating that the algorithm correctly identifies aircraft with high probability at the anticipated noise levels. Performance can be expected to decline as the noise power surpasses the maximum signal power.

I. Introduction

Two parallel schools of thought dominate the literature regarding the recognition of fast-moving fixed-wing aircraft. The first proposes a two-step approach to the problem. Target images are created, such as two-dimensional inverse synthetic aperture radar (ISAR) images or a sequence of one-dimensional range profiles [1]. Target recognition is then conducted using these images. The alternate approach has been to bypass the creation of images and attempt recognition directly from the received data. Herman [2], [3] takes this second approach to automatic target recognition (ATR), using data obtained from a passive radar system.

Although ATR has been a subject of much research, Herman's application of passive radar was innovative. Unlike traditional radar systems, passive radar systems bypass the need for dedicated transmitters by exploiting "illuminators of opportunity" such as commercial television and FM radio signals. In doing so, they are able to reap a number of benefits. Most notably, the fact that passive radar systems do not emit energy renders them covert. An additional benefit is that the illuminators of opportunity often operate at much lower frequencies than their traditional counterparts. These low-frequency signals are well-suited for ATR [4], [5], [6].

II. Approach

The primary goal of this research is to add ATR capabilities to existing passive radar systems, using RCS as the key information for classification. Since RCS is highly aspect-dependent, accurate estimation of target orientation is crucial. Herman [2], [3] met this challenge with a computationally intensive particle filter [7], which jointly estimated target position, orientation, and target type. This paper seeks a less computationally intensive approach. The positions and velocities estimated by the existing passive radar system are considered to be "true." They are then exploited by a coordinated flight model [8], [9] to estimate aircraft orientation.

A database of Fast Illinois Solver Code (FISC) results is created for each aircraft in the target class. This database is accessed using the aircraft orientations estimated by the coordinated flight model. This results in a set of power profiles simulating those that would arrive at the receiver if the aircraft in the target class were executing the maneuver. These profiles are then scaled for propagation losses and antenna gain of the receiver using the Advanced Refractive Effects Prediction System (AREPS) and Numerical Electromagnetic Code (NEC2), respectively. Finally, the profiles corresponding to members of the target class are compared to the profile of the actual target, resulting in target identification.

A secondary goal of this research is to model a system currently being developed by NATO/NC3A with the intent of an eventual comparison with real data. At this time, though, the research is purely simulation-based. It is worth noting that the aircraft comprising the target class have been chosen based upon the availability of

0-7803-8281-1/04/$20.00/

acceptable CAD models, rather than likelihood of occurrence near the NATO/NC3A system. This will change as a comparison with real data draws near. In the meantime, the target class is comprised of the F-15, T-38A, Falcon-20, and Falcon-100.

III. Modeling Target RCS

Given that target RCS is the sole factor used to classify the aircraft, its accurate representation is paramount. This task is not trivial, as RCS is heavily dependent upon the incident and observed angles, which in turn are dependent upon the yaw, heading, pitch, and roll of the aircraft. Our response to this challenge implements a coordinated flight model to estimate these angles, given a set of time-correlated aircraft positions. This process is described at length in other sources [8], [9]; thus, only the results will be presented here.

Since this research is primarily concerned with fast-moving fixed-wing aircraft, yaw is always assumed to be zero. Aircraft heading, a far more revealing parameter, is expressed as,

$$\xi = \begin{cases} 90 - \arctan(\frac{v_Y}{v_X}), x > 0 \\ 270 - \arctan(\frac{v_Y}{v_X}), x < 0 \end{cases}, \quad (1)$$

where v_X and v_Y are the x and y components of aircraft velocity. The equation of pitch also follows from the assumption that the aircraft nose is pointed in the direction of motion, and is expressed as,

$$\theta = \arctan\left(\frac{dz}{\sqrt{dx^2 + dy^2}}\right), \quad (2)$$

where (dx, dy, dz) is the difference in aircraft position in the x, y, and z directions over an incremental period of time, dt. Finally, the aircraft roll is estimated as,

$$\phi = \arctan\left(\frac{|v|^2 \cos(\theta)}{Rg}\right), \quad (3)$$

where $|v|$ is the magnitude of the aircraft velocity, R is the instantaneous radius of curvature of the aircraft turn, and g is the standard gravity at Earth's surface.

The estimated aircraft orientation angles are appended to the aircraft positions, creating a supplemented flight profile. This supplemented flight profile is then used to determine the incident and observed angles at every point during the encounter. These angles allow us to access a database of FISC results, which are available for each aircraft in the target class. A set of power profiles are created when data is extracted from the RCS database. Additional scaling is required to make these power profiles represent the signals arriving at the receiver due to the illuminated targets. Some significant factors that must be considered are propagation losses between the aircraft and antennas, and antenna gain. The propagation losses, which include effects due to multipath, are modeled using AREPS. As is likely to be the case for most passive radar applications, the transmitting antenna exploited by the NATO/NC3A system is omni-directional. Thus, the only antenna gain pattern that must be modeled corresponds to the receiver; this modeling is accomplished with NEC2. The overall result of this process is a power profile that is scaled to account for propagation losses and antenna gain.

Until real data is available from the NATO/NC3A system, it is also necessary to simulate the detected target power profiles. First, the simulation is run with the real aircraft orientations used in place of the estimated ones. These power profiles are then corrupted with additive white Gaussian noise, which acts independently on the real and imaginary parts of the signal. Along these lines, the simulated profile arriving at the receiver is expressed as,

$$P_{SIM} = (\sqrt{P_R} + w_R)^2 + w_I^2, \quad (4)$$

where P_R is the real component of the power profile prior to being corrupted by noise, and w is zero-mean additive white Gaussian noise, which has real and imaginary components, w_R and w_I [3]. The noise power is computed in dBW using,

$$P_N = \frac{kT_0N_F}{CPI}, \quad (5)$$

where k is Boltzmann's constant, T_0 is temperature in Kelvin, N_F is the unitless noise figure, and CPI is the coherent processing interval of the system [10]. To match the NATO/NC3A system, the CPI is set equal to 0.5 seconds, and T_0 is set equal to 290 K.

Selection of the noise figure, N_F, is more difficult. If the noise figure is only expected to account for thermal noise and out-of-band interference, then a conservative estimate of the noise figure in a city environment might be 30 dB. To be thorough, the noise figure is swept over a range of values, allowing us to quantify system performance as a function of noise power. The noise figures used in this paper range from 30 dB to 100 dB in increments of 5 dB. Note that noise figures above 30 dB are not expected to occur in a real setting; they are merely included in this paper to demonstrate the breaking point of the algorithm.

Thus far, the issue of transmitter interference has been neglected. Typically, this direct path interference manifests itself as a spike in the cross-ambiguity function. Since the transmitter's power and location are known, and since the direct path interference spike occurs along the axis with zero velocity, this spike can usually be identified and removed. The more treacherous effect of transmitter interference is that is can raise the "thumbtack" noise floor of the ambiguity function, potentially

masking the target spike. To be thorough, this should also be considered when computing the noise figure.

If the ambiguity function is normalized such that the direct path spike has unit height, then the average pedestal height, or sideband power, is given by

$$P_{pedestal} = \frac{1}{B \times CPI}, \tag{6}$$

where B is the signal bandwidth, and CPI is the coherent processing interval [11]. To match the NATO/NC3A system, values of 45 kHz and 0.5 seconds are used for B and CPI, respectively.

If propagation losses and antenna gain are neglected, the pedestal power is 44 dBW below the direct-path spike. Since the NATO/NC3A transmitter power is 50 dBW, the sideband power is 6 dBW. Propagation losses and antenna gain play a significant role, lowering the pedestal power by 95 dBW. The electronics in the receiver of the NATO/NC3A system also mitigate the problem by suppressing the direct path signal by 70 dBW, which reduces the sideband power to -159 dBW. More sophisticated filters could be implemented to further reduce the noise figure, but using the specifications of the system being modeled, the effective noise figure falls between 40 and 45 dB. Thus, the effects due to transmitter interference are far more significant than those due to thermal noise and out-of-band interference.

This underscores an important point. In the interest of gauging the algorithm's performance in the presence of noise, the results presented in Section V correspond to a broad range of noise figures. When reading that section, it is imperative to recall that the anticipated noise figure in the real system is only 40 dB.

IV. Target Identification

A set of detected target profiles is created for each aircraft in the target class. The automatic target recognizer compares these noisy profiles to the library of precomputed, noise-free profiles. Equation 4 leads to a Rician likelihood model [3] whose probability density function is given by

$$p_x(x) = \frac{x}{\sigma_w^2} e^{\left(\frac{x^2+s^2}{2\sigma_w^2}\right)} I_0\left[\frac{xs}{\sigma_w^2}\right]. \tag{7}$$

To apply the Rician, associate x with the profile from the detected target, and s with the precomputed, noise-free profile. The noise power, which equals the noise variance, is then equated with σ_w^2. If each point in time is considered an independent sample from a process, then the data loglikelihood is

$$\ln(p_x(\bar{x})) = \sum_{i=1}^{n} \ln\left(I_0\left[\frac{x_i s_i}{\sigma_w^2}\right]\right) - \left(\frac{x_i^2 + s_i^2}{2\sigma_w^2}\right). \tag{8}$$

Loglikelihoods are computed for each member of the target class; the target is identified as the member of the target class with the largest loglikelihood [12].

V. Results

A flight profile recorded on-board a maneuvering F-15 at Edwards Air Force Base[1] is used to provide a realistic test of the algorithm. The Edwards trajectory came complete with measured aircraft orientation, allowing a unique opportunity to quantify the performance degradation induced by the coordinated flight model. First, the algorithm is executed with the real aircraft orientation angles used in place of the ones estimated by the coordinated flight model. This serves as a baseline for comparison. Next, the simulation is run using the estimated aircraft orientation angles. A third test is conducted in which the aircraft position is errantly estimated to be 300 m north and 300 m west of its actual location. This gauges performance degradation due to errors in the position estimates.

The aircraft remains in the receiver's main lobe throughout each engagement, and is located approximately 79 km from the transmitter and 25 km from the receiver. During the maneuver, the target changes altitudes and executes turns with varying degrees of curvature. This maneuver is shown in Figure 1 from both 3-D and 2-D perspectives.

The approach described in Section III is implemented; the noise figure is swept from 30 dB to 100 dB, in increments of 5 dB, to gauge performance degradation of the algorithm as a function of noise level. One-hundred runs are executed using each aircraft as the detected target, for each noise figure. The percentage of incorrect identifications (probability of error) obtained for the F-15 under the three sets of tests are shown in Figure 2b. This data is obtained from a set of Monte Carlo runs; thus the jumps in the curves are artificial and are expected to smooth out as the number of samples increase.

The power profiles generated for the F-15 under the three different tests are shown in Figure 2a. Although the power profiles show some marked deviations when the orientation angles are estimated and when the position errors are included, the probability of error curves corresponding to the three tests are remarkably similar. In fact, there seems to be little degradation in performance due to using the coordinated flight model, even in

[1]The F-15C trajectory was obtained from the Joint Helmet Cuing System, Mission JH-16, conducted by the 445th Flight Test Squadron at Edwards Air Force Base in May 2000.

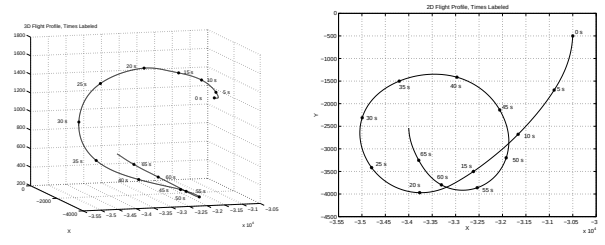

Figure 1. F-15 maneuver: a) 3-D view (left), b) top view (right).

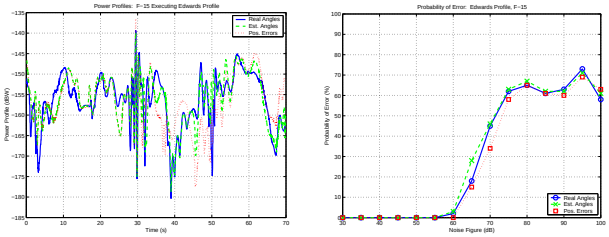

Figure 2. F-15 executing the Edwards trajectory: a) power profiles (left), b) probability of error (right).

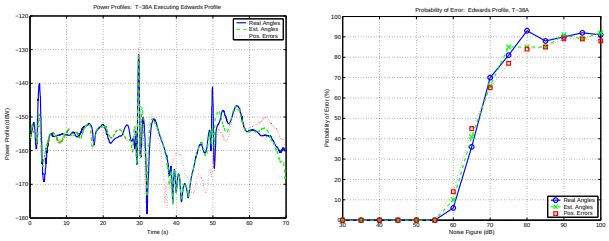

Figure 3. T-38A executing the Edwards trajectory: a) power profiles (left), b) probability of error (right).

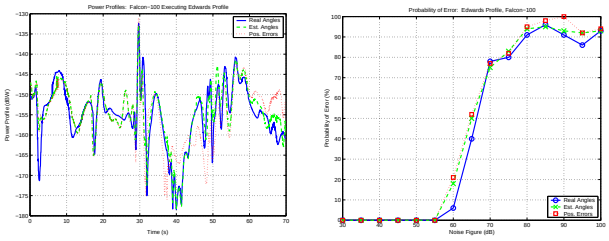

Figure 4. Falcon-100 executing the Edwards trajectory: a) power profiles (left), b) probability of error (right).

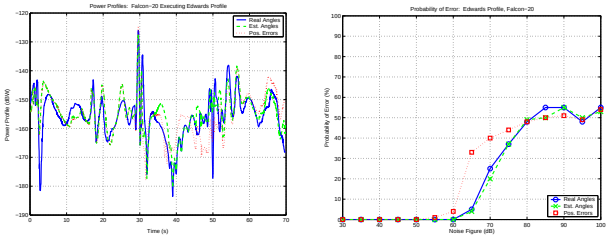

Figure 5. Falcon-20 executing the Edwards trajectory: a) power profiles (left), b) probability of error (right).

the presence of position errors. This is also true for the T-38 and Falcon-100, whose plots are shown in Figures 3 and 4, respectively.

The only aircraft for which degradation in performance is noted is the Falcon-20. Even in this case, the performance is nearly identical when the estimated orientation angles are substituted for the actual ones. The only performance degradation occurs when the errant positions are used to estimate the orientation angles. The power profiles and probability of error plots for the Falcon-20 appear in Figure 5. Note that in every one of these simulations, the algorithm performs extremely well at the anticipated noise figure of 40 dB.

Confusion matrices are tabulated to provide insight into the nature of the algorithm's errors. The confusion matrices obtained with a noise figure of 65 dB are shown in Tables 1 through 3. The aircraft listed in the first column correspond to the aircraft detected by the receiver. The aircraft listed across the top row pertain to the aircraft identified by the algorithm. To get a better sense of the differences in algorithm performance between the three tests, we computed the percentage of total errors. For a noise figure of 65 dB, the algorithm is correct 75% of the time when the orientation angles are known, 69% of the time when the orientation angles are estimated from correct positions, and 64% of the time when incorrect position estimates are used.

Table 1. Confusion matrix for the Edwards trajectory with noise figure = 65 dB, using real orientation angles.

Aircraft	F-15	T-38A	Falcon-20	Falcon-100
F-15	82	8	0	10
T-38A	13	64	2	21
Falcon-20	0	3	95	2
Falcon-100	17	21	2	60

Table 2. Confusion matrix for the Edwards trajectory with noise figure = 65 dB, using estimated orientation angles.

Aircraft	F-15	T-38A	Falcon-20	Falcon-100
F-15	72	14	1	13
T-38A	16	59	5	20
Falcon-20	0	3	96	1
Falcon-100	15	29	6	50

VI. Summary

Passive radar is an emerging technology that is only beginning to be exploited by the scientific community. The addition of ATR capabilities can only enhance the effectiveness of these systems. While this task was attempted by Herman with a particle filtering scheme, the major

Table 3. Confusion matrix for the Edwards trajectory with noise figure = 65 dB, using incorrect position estimates.

Aircraft	F-15	T-38A	Falcon-20	Falcon-100
F-15	85	6	0	9
T-38A	25	55	0	20
Falcon-20	0	15	67	18
Falcon-100	25	27	0	48

contribution of this paper is that it demonstrates that good results are often possible with a simpler approach.

In this case, we are able to show via simulations that excellent ATR results are possible at the anticipated noise levels, through the coupling of a coordinated flight model and RCS database. The ATR performance degrades as the noise level increases, indicating that the algorithm would be less successful identifying aircraft that are not sufficiently within the receiver's main lobe, or that are not sufficiently close in range to the receiver. The range required to generate sufficient SNR for reliable identification is dependent upon the target type and orientation.

It is worth noting that preliminary findings using the same maneuver and horizontally polarized transmitters and receivers are not as encouraging. Future work will address the derivation of performance bounds for both cases, and will seek a more robust classification algorithm by jointly estimating target type and orientation. Additional plans for future work include expansion of the FISC database via sparse sampling techniques.

VII. Acknowledgements

This work was funded by the NATO Consultation, Command, and Control Agency (NC3A), as well as by start-up funds from the School of Electrical and Computer Engineering at the Georgia Institute of Technology. The authors would like to thank Dr. Paul Howland and Dr. Rene van der Heiden at NC3A for their support. They would also like to thank Major Larkin Hastriter and Lt. Col. Adam MacDonald for their assistance in obtaining aircraft flight paths. Finally, the authors would like to thank Professor Lakshmi Sankar of the School of Aerospace Engineering at the Georgia Institute of Technology for his patience and guidance.

References

[1] S.P. Jacobs and J.A. O'Sullivan, "Automatic target recognition using sequences of high resolution radar range-profiles," *IEEE Trans. on Aerospace and Electronic Systems*, vol. 36, no. 2, pp. 364–382, 2000.

[2] S.M. Herman, *A Particle Filtering Approach to Joint Passive Radar Tracking and Target Classification*, Doctoral Dissertation, Department of Electrical and Computer Engineering, Univ. of Illinois at Urbana-Champaign, Urbana, IL, 2002.

[3] S.C. Herman and P. Moulin, "A particle filtering approach to joint radar tracking and automatic target recognition," in *Proc. IEEE Aerospace Conference*, Big Sky, Montana, March 10-15 2002.

[4] Y.T. Lin and A.A. Ksienski, "Identification of complex geomtrical shapes by means of low-frequency radar returns," *The Radio and Electronic Engineer*, vol. 46, no. 10, pp. 472–486, Oct. 1976.

[5] H. Lin and A.A. Ksienski, "Optimum frequencies for aircraft classification," *IEEE Trans. on Aerospace and Electronic Systems*, vol. 17, no. 5, pp. 656–665, Sept. 1981.

[6] J.S. Chen and E.K. Walton, "Comparison of two target classification techniques," *IEEE Trans. on Aerospace and Electronic Systems*, vol. 22, no. 1, pp. 15–21, Jan. 1986.

[7] A. Doucet, N. de Freitas, and N. Gordon, *Sequential Monte Carlo Methods in Practice*, Springer-Verlag, 2001.

[8] L. Ehrman and A.D. Lanterman, "Estimation of aircraft orientation from flight paths using a coordinated flight model," *submitted to IEEE Transactions on Aerospace and Electronic Systems*, November 2002.

[9] L.M. Ehrman, *Automatic Target Recognition Using Passive Radar and a Coordinated Flight Model*, Master's Thesis, School of Electrical and Computer Engineering, Georgia Institute of Technology, Atlanta, GA, 2004.

[10] D.K. Barton, *Modern Radar System Analysis*, Artech House, 1988.

[11] M. A. Ringer, G. J. Frazer, and S. J. Anderson, "Waveform analysis of transmitters of opportunity for passive radar," *Surveillance Systems Division, Electronics and Surveillance Research Laboratory.*

[12] L. Ehrman and A. Lanterman, "Automated target recogntion using passive radar and coordinated flight models," in *Automatic Target Recognition XIII*, Orlando, FL, April 2003, vol. SPIE Proc. 5094.